Deanship of Graduate Studies
Al- Quds University

Evaluation of Organs Absorbed Doses, effective doses and Cancer risk Following Chest HRCT Scan for COVID-19 Patients

Hala Yousef Hussein Dar Rabee

M. Sc. Thesis

Jerusalem – Palestine

1445/ 2024

Evaluation of Organs Absorbed Doses, effective doses and Cancer risk Following Chest HRCT Scan for COVID-19 Patients

Prepared by:
Hala Yousef Hussein Dar Rabee

B.Sc in Medical Imaging Technology, Department of Medical Imaging/Al-Quds University/ Jerusalem-Palestine

Supervisor: Dr. Mohammed Al Hjouj

A thesis Submitted in Partial Fulfillment of Requirements for a Master degree in Medical Imaging Technology. Faculty of Medical Imaging/Al-Quds University

1445 / 2024

Al- Quds University

Deanship of Graduate Studies

Medical Imaging Technology

Thesis Approval

Evaluation of Organs Absorbed Doses, effective doses and Cancer risk Following Chest HRCT Scan for COVID-19 Patients

Prepared by: Hala Yousef Hussein Dar Rabee

Registration No: 21811023

Supervisor: Dr. Mohammed Al-Hjouj

Master thesis Submitted and Accepted: 24/5/2024

The names and signature of the examining committee members are as follows:

1. **Head of Committee: Dr. Mohammad Hjouj Signature**
2. **Internal Examiner: Dr. Hussein ALMasri Signature** Hussein ALMasri
3. **External Examiner: Dr. Samer Muhanna Signature**

Jerusalem – Palestine

1445 / 2024

Dedication

In the hopes that this work will contribute to avoiding harm to patients, this work is dedicated to my beloved brother Hussein who always gave his support to me before he left, will be in my memory.

Hala Yousef Hussein Dar Rabee

Declaration

I certify that this thesis submitted for the degree of master, is the result of my own research, except where otherwise acknowledged, and that thesis has not been submitted for a higher degree to any other university or institution.

signed 

Hala Yousef Hussein Dar Rabe

Date: 24/5/2024

Acknowledgement

First and foremost, I'd like to thank God for assisting me in continuing my scientific career.
Thanks to my supervisor Dr. Mohammed Al-Hjouj
Great thanks to Dr. Huda Dahbour my mother-in-law who supported me during this journey.
The greatest thanks to my husband for giving me all the inspiration and support I need.
Many thanks to my parents and family.

Hala Yousef Rabee

Evaluation of Organs Absorbed Doses, effective doses and Cancer risk Following Chest HRCT Scan for COVID-19 Patients

Abstract

CT imaging is an effective modality for diagnosing a wide range of medical conditions. CT outperforms x-rays in terms of 3D image generation and soft tissue visualization. CT imaging of the lungs is an important diagnostic tool in the fight against pneumonia. The use of the HRCT imaging protocol for the chest has increased during the COVID-19 pandemic. It is possible to use CT scans for both diagnostic and screening purposes. Radiation risk must be considered, and the dosimetric effects of chest HRCT must be assessed. CT imaging could assist with the early detection of COVID-19-related interstitial pneumonia. There is no agreement on the use of CT for diagnosis due to the first stage of the disease can be negative.

So, this study aims to evaluate the dosimetric impact of HRCT of the chest for COVID-19 Patients. The mean organ and effective doses will be evaluated. Also, estimation of radiation cancer risk in (lung, stomach, colon, thyroid, and breast) associated with these exposures according to the Biological Effects of Ionizing Radiations (BEIR) VII report.

The study's goal was achieved through the use of quantitative retrospective cohort analysis. The study population consists of 49 adult patients (31 males and 17 females), aged 18 to 89 years, who underwent HRCT during the period between April 26th, 2020, and March 20th, 2021. Data was collected using a local picture archiving and communication system (PACS), including patient demographics and anthropometrics, as well as dose descriptive information (CTDIv and DLP). The effective dose was calculated using two methods: first, using the tissue conversion coefficient (k) for the chest CT, and second, using the VirtualDose™ CT software, which also calculates the organ absorbed dose. The software is based on a large database of organ doses generated via Monte Carlo (MC) simulations using a library of 25 anatomically realistic phantoms. Then The life time attributable risk (LAR) of developing cancer in a specific organ (T) was determined by risk coefficients obtained from Biological Effects of Ionizing Radiations (BEIR) VII report. Each dosimetric parameter is defined by its mean, median, standard deviation, and 75th percentile. We used the MV for comparing our results with previously reported values. The mean value of equivalent doses and the cancer risk probability for organs have been established for either or both gender groups.

Spearman's rank-order test was used to test for correlations between, DLP\BMI, ED_{DLP}, and ED_{MC}. The significance level was defined as $p < 0.05$. The results of the study revealed that the average calculated effective dose for total population 9.7 mSv, and the average effective dose estimated by virtual dose CT software was 13.47 mSv, with female average dose higher than male with a value of 14.75 and 12.7 mSv respectively. The result showed a decreased effective dose for patients with increased patient BMI while increased with increased DLP. Females

showed a higher organs dose than males for all organs as well as cancer risk except for colon, the highest risk were found in lungs for both gender as it 51.6 per 100.000 for females and 21.8 per 100.000 per males.it was concluded that the current chest HRCT protocol result in significant radiation doses to the patients compared to reported in previous studies.

Table of contents

List of Tables:

List of Figures

List of Abbreviations and Units

Abbreviation	Meaning
CT	Computed tomography
MDCT	Multidetector-row computed tomography
MRI	Magnetic resonance imaging
3D	Three-dimensions
2D	Two-dimensions
HRCT	High resolution computed tomography
cm	Centimeters
mAs	Milliampere /second
KVP	Kilo voltage peak
SARS-CoV-2	severe acute respiratory syndrome corona virus 2
COVID-19	Coronavirus disease 2019
WHO	World Health Organization
°C	Celsius
(RT-PCR)	Real-time reverse transcription polymerase chain reaction
mSv	Millisievert
ED	Effective dose
DNA	Deoxyribonucleic acid
BEIRVII	Biological effects of ionizing radiation report VII
ICRPI	International Commission on Radiological Protection
GE	General Electric
μ	The linear attenuation coefficient
HU	Hounsfield Units
kW	Kilowatts
AEC	Automatic exposure control
P	Pitch
D_T	Organ absorbed dose
Gy	Gray

H_T	Organ Equivalent dose
W_R	Radiation weighting factors
W_T	Tissues weighting factor
$CTDI_V$	CT dose index volume
$CTDI_W$	CT dose index
DLP	Dose length product
mGy.cm	Milli-gray. centimeters
DICOM	Digital Imaging and Communications in Medicine
RDSR	Radiation Dose Structured Report
PACS	Picture archiving and communication system
BMI	Body mass index
LAR	Lifetime attributable risk

Chapter One

Introduction

This chapter discusses the background of the study, problem statement, justification, study objectives, and the hypothesis.

1.1 Introduction

Since 1895 when X-rays were discovered by a German physicist Wilhelm Conrad Rontgen, a revolution in the medical field has occurred, when x-rays allow for the first time to look inside the patient noninvasively, it became a worldwide basic imaging diagnostic tool, advances in the medical imaging field continued until the 1972 a turning point happened in this field when Godfrey Newbold Hounsfield combined digital computer system with x-ray source, which implemented the first computerized x-ray imaging modality, computed tomography (CT), or refers to computed axial tomography (CAT)(Cantatore et al. 2011). This cross-sectional imaging modality had a fundamental impact on the field of medicine and became a basic diagnostic tool worldwide, also with the improvement of machine instrumentations including the hardware and software led to the development of seven generations of CT scanners during the past four decades, which varies in the characteristics of the CT image based on the arrangement and the movement of the x-ray tube and detectors, the newest breakthrough in CT is the multidetector-row computed tomography (MDCT), which transformed CT technology in a real three-dimensional imaging technique offered a variety of advantages such as short scan time and longer scan ranges than the other generations(Marchal et al. 2005). CT imaging is considered a powerful modality helping multiple imaging protocols in the diagnosis of many medical conditions such as cancer, trauma, lung disease, heart disease, and musculoskeletal disorders, whin compared the CT scan to other imaging modalities conventional x-ray and magnetic resonance imaging (MRI) we conclude that CT has strengths points over x-ray regarding the creation of three dimensional (3D) images in CT rather than (2D) images in x-ray and better visualization of soft tissues, also it offers better visualization of bones than MRI dose in addition to the faster scan time and the simpler performance and interpretation (Marchal et al. 2005)

One of the important CT imaging protocols of the lung is the high-resolution computerized tomography of the lung (HRCT).In patients suffering from diffuse lung disease, for instance idiopathic interstitial pneumonia, emphysema, and others, this scan play a critical role in forming an initial diagnosis(Elicker et al. 2017), HRCT has a higher spatial resolution than conventional CT, allowing for a better assessment of parenchymal detail, it can detect

pneumonia about 5 days earlier than when chest radiographs are used exclusively in patients with the histologically proven disease when the sensitivity of HRCT is compared to the sensitivity of the chest radiograph in these patients, the average sensitivity is found to be 80% for a chest x-ray and 94% for HRCT which essentially eliminates the superimposition effects that have traditionally made the chest radiograph ineffective (Padley et al.1995). HRCT is a technique that combines thin collimation scans with a high spatial frequency algorithm, such as the bone algorithm, to sharpen the resolution of thin structures and improve fine image detail(Corcoran et al.1992). HRCT can be done in two ways: the older spaced axial or volumetric scans. The former is done at 0.5 to 2 cm intervals and provides an adequate sampling of the lung parenchyma that is representative of the overall process, as well as an incremental reduction in the radiation dose compared to volumetric imaging since the entire lung is not included.
Volumetric imaging, on the other hand, is superior in its adequacy and accuracy when the entire lung is imaged with a contiguous scan, slight changes in disease degree are easier to detect, while spaced axial images sample only 20-25% of the chest(WHO) can severely restrict longitudinal changes and overlook focal anomalies like pneumonia(Elicker et al. 2017). Volumetric or contagious thin collimation HRCT of the entire lung cannot be done with single-slice helical CT because it is difficult to achieve in a single breath-hold(Schoepf et al. 2001), multidetector-row computed tomography that has been introduced recently in clinical practice can easily obtain contiguous thin-slice images of the entire lungs in just one breath hold in a short time (MDCT)(Schoepf et al. 2001; Yanagawa et al. 2018). MD-HRCT should be used with caution due to the increased radiation dose involved, especially since the radiation exposure factors, such as mAs and kVp differ between scanners ranging between low to high radiation doses(Wolters 2014).

Recently chest HRCT has played a vital role when an outbreak of pneumonia of unknown etiology was identified in Wuhan, China, in December 2019, the pathogen was a novel coronavirus related to the novel severe acute respiratory syndrome coronavirus 2 (SARS-CoV-2) and termed later as coronavirus disease 2019 (COVID-19) by the World Health Organization (WHO)(Alam et al. 2020), the symptoms of COVID-19 are ranging from mild (fever, dry cough, and fatigue) to severe symptoms such as Shortness of breath, loss of appetite, Confusion, Persistent pain or pressure in the chest and High temperature (above 38 °C). The virus originated in bats and was transmitted to humans through yet unknown intermediary animals in Wuhan(Singhal 2020), The virus is human-transmittable and has sparked a worldwide pandemic, this new coronavirus spreads primarily through respiratory droplets produced when infected individual coughs or sneezes(Alam et al. 2020), people over the age of 60, as well as those with underlying medical conditions such as high blood pressure, heart and lung disease, diabetes, obesity, or cancer, are at a higher risk of developing serious illness such as interstitial pneumonia, however, someone of any age may become ill with COVID-19 and become severely ill or die(WHO.2023) The coronavirus COVID-19 affects 219 countries and territories, by 18-3-2021, the number of cases had risen to 121,921,932 worldwide, including 2,694,702 death cases while 98,260,551 cases were recovered(METER 2021). Rapid and reliable COVID-19 identification is critical for controlling outbreaks in the population and in hospitals, the respiratory tract specimens were gathered for analysis using either next-generation sequencing or real-time reverse transcription-polymerase chain reaction (RT-PCR), resulting in sensitivities that vary between 60% to 71% ,which is the gold standard for the diagnosis of SARS-CoV-2 infection(Ghetti et al. 2020), while several studies found that using a CT scan of the chest to diagnose COVID-19 pneumonia had a high sensitivity (around 97%) since it is very sensitive to

the primary imaging features in the COVID-19 pneumonia which is ground-glass opacity, while recent guidelines show that there is not a consensus on the use of CT for COVID-19 diagnosis since it may be negative in the early stages of the disease

In addition to the cost and radiation exposure(Ghetti et al. 2020), however, the HRCT Chest is an effective method for both diagnosis and management of patients with COVID-19, and an important complement to the RT-PCR tests(Alam et al. 2020). On the other hand, the impressive increase of HRCT scans during the COVID-19 pandemic could lead to a dosimetric consequence since the involvement of ionizing radiation which, has a biological effect on patients.

1.2 Problem Statement

Computerized Tomography (CT) has become a common technique in medical imaging departments due to its ability to produce highly detailed images quickly, and the various imaging protocols it provides. The urgent need for an alternative diagnostic than RT-PCR kits has given rise to the possibility of utilization of chest CT findings as a diagnostic aid and a screening tool in suspected patients. The use of HRCT imaging protocol of the chest has increased during the COVID-19 pandemic, which plays a critical role in the management of this global health emergency. However, a balance must be struck between obtaining adequate diagnostic information and patient safety, since exposure to ionizing radiation results in the ionization of atoms, which can result in cell impairment or death depending on the irradiation's intensity.

At high doses (above 100 mSv), the effect is immediate and certain in the event of subsequent exposure to a higher dose greater than the impact threshold, this is referred to as deterministic effect(BEIR 2006, Antoni et al. 2017). In diagnostic medical imaging the exposure to low doses (below 100 mSv), leads to a stochastic effect in which the effect is delayed and does not necessarily manifest itself in each person who is irradiated, it is a stochastic process for which there is no known threshold of occurrence, cancer induction is the most common late effect of radiation(BEIR 2006; Antoni et al. 2017). Replacing conventional CT (CCT) with low-dose CT (LDCT) and ultra-low-dose CT (ULDCT) has been proposed as a method to decrease radiation exposure in these patients(Tofighi et al. 2020), the objective of LDCT scanning is to preserve good image resolution while minimizing radiation by optimizing scanning settings and utilizing an iterative reconstruction algorithm as iterative reconstruction techniques can reduce dosage by up to 62 percent(Finance et al. 2021). Unfortunately, the present protocol of HRCT is still the same. So, it’s important to keep in mind that the radiation risk must be considered and the dosimetric impacts of chest HRCT must be evaluated.

1.3 Justification

CT imaging may aid in the initial identification of COVID-19-related interstitial pneumonia patients. The most recent recommendations demonstrated that there is no consensus on the application of CT for COVID-19 diagnosis because it may be negative in the early stages of the disease. (Revel et al. 2020)

This remarkable and unexpected rise in this screening examination may have dosimetric consequences for patients, so low dose protocols for chest CT in patients suspected of COVID-19 pneumonia should be considered. There is concern that prolonged exposure to the ionizing radiation of CT could boost the risk of acquiring solid malignancies, and leukemia(Berrington De González et al. 2009). The HRCT protocol is still being used without any modification in image-related acquisition parameters. The need to support local governmental and other private hospitals in their response to the COVID-19 pandemic in patients with suspected or confirmed COVID-19 by using HRCT protocol is essential to demand. This guide is expected to promote the quality and safety of radiation used in health facilities, thus enhancing the protection and safety of patients and health workers. It is not intended to replace clinical judgment or specialist consultation but rather to support care providers for the clinical management of these patients.

Since the COVID-19 pandemic is recent there are no diametric studies on COVID-19 patients who were imaged by a high dose chest HRCT scan protocol. Lack of knowledge about the radiation risks induced by high dose HRCT as the parameters are still the same is another concern. However, a related analysis was conducted on low-dose chest HRCT protocol.

1.4 Study Objectives

This study aims to evaluate the dosimetric effects of HRCT for COVID-19 Patients. With this, both mean organ and effective doses will be assessed.

Also, estimation of radiation cancer risk in (lung, stomach, colon, thyroid, and breast) associated with these exposures according to Biological Effects of Ionizing Radiations (BEIR) VII report(BEIR 2006)

1.5 Study Hypothesis

The variations in average effective doses (ED) values between those tested in Palestine and those reported globally would be intolerable.

Chapter Two

Literature Review

This chapter summarizes the basic principles of computed tomography, radiation dosimetry in CT as well as previous studies related to the ionizing radiation risk, radiation dose in HRCT, and a recommended HRCT technique during the pandemic.

2.1 Scientific Principles of Computed Tomography

2.1.1 Overview:

The key benefits of computed tomography compared with conventional radiographs are the absence of the superimposed structures since the conventional method display a two-dimensional representation of a 3D object, and the ability of CT scans to discern minor variations in the density and anomalies of anatomical structures moreover a superior image quality as CT use a narrow rotating x-ray beam to scan a thin section of the body(ROMANS 2011)

2.1.2 Terminology:

The word tomo in tomography is derived from Greek tomoes which means to cut, layer, or section. CT involves a complex computerized approach, which utilized for collect data and transform them into 'cuts.' or cross-sectional slices of the human anatomy, the term computerized axial tomography (CAT) referred to the older scanning system which was limited to the production of only axial cross-section images, The term "axial" has been removed from the name of the CT equipment because modern versions provide a greater variety than just axial cuts. While every CT manufacturers started in the identical fundamental shape, they attempted to distinguish their scanners in the market by incorporating characteristics and functions into the current technology, so depending on the manufacturer, the same feature or function has a range of different names, for example, “topogram” (Siemens), “scout” (GE Healthcare), or “scanogram” (Toshiba) these all are terms referred to the preliminary image which every scanner produces, also the continuous acquisition scan method, identified as a "spiral" (Siemens), "helical" (GE healthcare) or "isotropic" (Toshiba) scanning(ROMANS 2011). The quality of CT image is usually assessed using several criteria as follows: (ROMANS 2011)

- Spatial resolution describes a system's ability to clearly define small objects.

- Low contrast resolution refers to a system's ability to differentiate objects with similar densities on the image.
- Temporal resolution refers to the speed of data acquisition.

2.1.3 The Essence of Computed Tomography:

CT employs a computer to process measurements obtained from the passage of ray beams in an anatomy area, and creates cross-sectional images, the CT slice only shows those portions of the anatomy at a specific level and indicates a particular plane in the patient's body, the thickness, width, and height of the plane are indicated by the three-axis Z, X and Y respectively the information and facts that represent the CT slice is divided into components: a picture element known as a pixel, which is a two-dimensional element (x,y), and a volume element known as a voxel, which is a three-dimensional element that includes the z-axis.

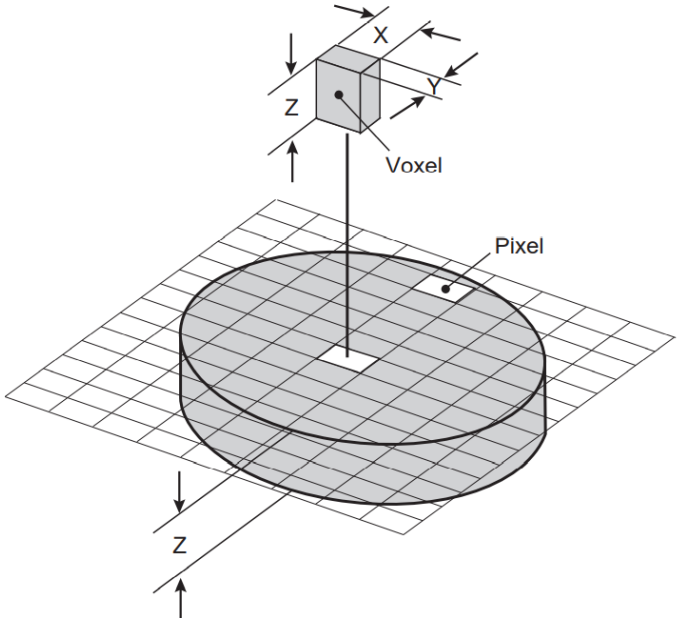

Figure 2.1: The data that comprise the CT slice are divided into elements.

2.1.4. Beam Attenuation:

An x-ray beam is made up of energy bundles known as photons. These photons may pass through or be redirected (i.e., scattered) by a structure, or they may be absorbed in varying amounts by a given structure depending on the intensity of the x-ray beam and the properties of the object (density, atomic number, and thickness) in its path.

The reduction of an x-ray beam's intensity as it passes through matter is known as attenuation, absorption, or deflection (scatter) of photons from the beam can both cause the reduction. An object's attenuation level determines which shades of gray it will be represented in on a CT image, in low attenuation material the x-ray photons will pass through without being obstructed so it will appear as a black area on the image, in contrast, a high attenuation material which can absorb most of the x-ray photons will appear as a white area on the image, while areas of different shades of gray on the image represent materials of intermediate attenuation levels. The linear attenuation coefficient (μ), expresses the percentage of the amount of x-rays redirected or absorbed per unit thickness of the an absorber, for instance, the linear attenuation coefficient for water at 125 kVp x-ray beam is about 0.18 cm−1 (the unit cm−1 donates per centimeter). This means that around 18% of the photons are absorbed or scattered when the x-ray beam passes by 1 cm of water, at the same magnitude of the x-ray beam, dense bone has the highest linear attenuation coefficient (0.46 cm-1) while (0.0003 cm-1) for air(ROMANS 2011).

The attenuation coefficient declines as photon energy evolves, and raises as atomic numbers and density increases, as many circulatory electrons and heavy nuclei are present providing more photon-interaction possibilities than less dense elements.

In the CT image, the distribution of the linear attenuation factor is directly demonstrated, indicating that variations in linear tissue attenuation coefficients contribute for the contrast of the X-ray image. To distinguish an object in a CT image from nearby objects, a density difference between the two objects is required; oral or intravenous contrast substances are frequently used to create a temporary difference between objects.

2.1.5 Hounsfield Units:

In CT, the attenuation capability of an object is better quantified than in conventional x-ray imaging. Measurements are expressed as CT numbers or Density values named Hounsfield Units (HU) **Fig. (2.2),** named after Godfrey Hounsfield.

Hounsfield assigned 0 to distilled water. The number 1000 was assigned to dense bone and -1000 was assigned to air. Objects with less beam attenuation than water have a negative number associated with this. Conversely, Hounsfield has a proportionately positive value for substances with an attenuation greater than that of water. The Hounsfield unit of anatomical structures that occur naturally is between 1000 and -1000. The unit value Hounsfield is directly associated with the linear attenuation ratio: 1 HU corresponds to a 0.1% difference between the attenuation coefficient of the tissue and that of the water therefore, a measurement of an undetermined structure appearing on an image is carried out using the system of Hounsfield unit and compared with measurements of previously identified structures, the composition of the unknown structure can then be approximated(ROMANS 2011).

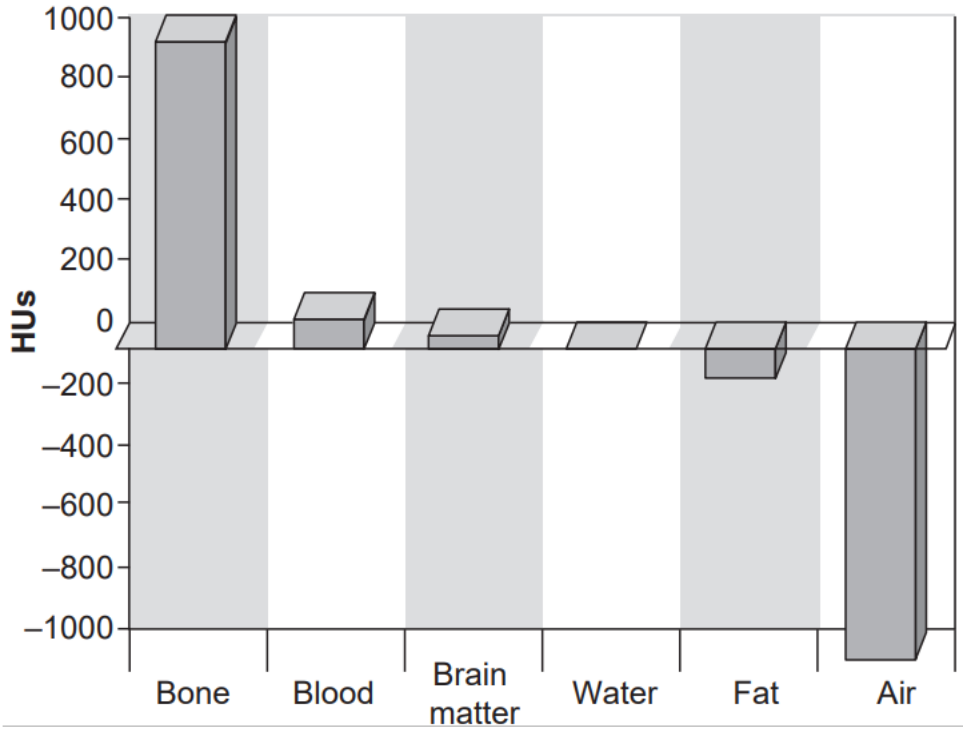

Figure 2.2: Approximation of Hounsfield Units

2.1.6 Scan Modes:

2.1.6.1 Conventional Axial Scanning:

Axial scanning, conventional scanning, serial scanning, sequence scanning, or step-and-shoot scanning are all terms that apply to the older, traditional form of scanning. The most important feature of this method is that the CT table is moved to the desired position and then remains fixed while the x-ray tube rotates inside the gantry, collecting data. The step-and-shoot technique generates radiographs that are perpendicular to the z-axis and analogous to the following slice, axial slices may be designed to acquire data in contiguous, gapped, or overlapping sequences depending on the slice increment(ROMANS 2011).

2.1.6.2 Helical Scan:

Helical CT has fundamentally changed diagnostic imaging since its launch in the late 1980s. Helical scanning, also known as spiral (or continuous acquisition) scanning, significantly increased scanning speed by eliminating the interscan delay. A helical scan method is described by three fundamental components: a continuously revolving x-ray tube, constant x-ray production, and continual table movement, adaptations of helical technology have been made to third-generation rotate-rotate CT scanner (which include multiple detectors up to 700 positioned in an arc) as well as to the fourth-generation rotate-fixed scanners (including a higher number of detectors up to 7,800 arranged in a ring. Initially, helical scanners had a

single row of detectors. Since then, MDCT systems have evolved such that used in this study(ROMANS 2011).

2.1.7 Major Components of CT System:

2.1.7.1 Gantry:

Many of the gadgets used for producing and analyzing x-rays can be found on the gantry. A circular rotating scan framework is used to position the components.

2.1.7.2 Slip Ring:

Slip rings allow continuous rotation of the gantry frame, enabling helical scan modes.

2.1.7.3 Generator:

Generate and relay high voltage to the x-ray tube. The generator's power output is measured in kilowatts (KW). The power capacity of the generator determines the variety of exposure techniques (kV and mA parameters).

2.1.7.4 Cooling Systems:

The gantry is equipped with cooling mechanisms. They come in a variety of shapes and sizes, including blowers, filters, and devices that conduct oil-to-air heat exchange. Cooling mechanisms are critical since temperature fluctuations can affect many imaging components.

2.1.7.5 X-ray Tube:

CT images are generated by x-ray photons produced and emitted by x-ray tubes.

2.1.7.6 Filtration:

Due to the polychromatic nature of the radiation released by CT x-ray tubes, filtering the x-ray beam helps to reduce the patient's radiation exposure and enhances image quality.

2.1.7.7 Collimators:

Collimators concentrate the x-ray beam on a particular location, reducing scattered radiation, increasing contrast resolution, and lowering the patient dose, Collimators regulate the thickness of the slices by constricting or expanding the x-ray beam.

2.1.7.8 Detectors:

Determine the intensity of x-ray radiation released along a beam projected from the x-ray tube to that particular detector component.

2.1.7.9 Patient Table:

The individual being examined will be set on the table (or couch, as some manufacturers define it) and moved into the gantry for the scanning process.

2.1.7.10 Computer System:

Before data, the acquisition is used for initiating the scan by adjusting many scan parameters, while after the data acquisition process the collected data from the detectors which refer to raw data is processed to generate an image using image reconstruction techniques and reconstruction algorithms such as iterative algorithms and filtered back projection.

2.1.8 Scan Parameters:

CT scan parameters influence both image quality and radiation dose.

2.1.8.1 Milliampere/ Second:

Milliampere-seconds (mAs) is the combination of milliampere setting and scan time and is used to quantify the x-ray beam. Additionally, it is known as tube current, mAs increasing resulting in improved image quality by improving signal to noise ratio (SNR) and noise reduction but increased the patient radiation dose.

2.1.8.2 Tube Voltage:

The term "peak kilovoltage" (kVp), refers to the highest voltage applied through an X-ray tube, which speeds up electrons from the cathode to the anode and thus determines the standard energy (quality) of the x-ray beam, radiation dose proportional to the square change in tube voltage.

2.1.8.3 Automatic Exposure Control (AEC):

Automatic Tube Current Modulation, which is software that automatically changes the tube current (mAs) to target specific anatomic areas, charging for significant differences in x-ray attenuation, and state a dose reduction of 15% to 40%(ROMANS 2011).

2.1.8.4 Slice Thickness:

Thinner slices provide a clearer image, improving the image's spatial resolution and reducing the signal-to-noise ratio, which requires a higher radiation dose to maintain a constant noise level.

2.1.8.5 Pitch:

Pitch (P) is described in the era of multidetector spiral CT as Table motion for each spin divided by the beam collimation, inversely proportional to radiation dose.

2.1.8.6 Scan Range:

Defines the region inside the gantry for which raw data is to be acquired, to prevent an unnecessary radiation dose, the scanned volume must be constrained to the region of interest, as the radiation dose is linearly proportional to the length scanned in the patient.

2.1.8.7 Increment:

Refers to the table/movement scanners to scan the next slice.

2.1.8.8 Reconstruction Algorithms:

Diverse CT scanners employ a variety of different reconstruction algorithms. Each of these algorithms provides for a variety of dose reductions; the ideal protocol, on the other hand, utilizes an efficient filter with the lowest radiation dose possible for the tissue type.

2.1.8.9 Rotation Time:

Denotes the time taken for the X-ray tube to rotate 360 degrees, directly proportional to the radiation dose.

2.2 Radiation Dosimetry in CT

Dosimetry is concerned with the quantification of the absorbed dose accumulated in the matter because of ionizing radiation, several dosimetric/protection quantities are used to measure the stochastic risks associated with ionizing radiation exposure.

2.2.1 Organ Absorbed Dose:

The dose applied to an organ or tissue on an average basis (DT), is defined in gray (Gy).

2.2.2 Organ Equivalent Dose:

To adjust the organ absorbed dose for the "typology" of radiation, the ICRP developed a concept called "equivalent dose in a tissue or organ, $H_{T,\,R}$ for a radiation R, by applying radiation weighting factors (W_R) to the organ absorbed dose-dependent on the type of radiation as the following equation (Antoni and Bourgois 2017).

$$H_{T\,(Sv)} = W_R\, D_{T,\,R} \quad \ldots\ldots (1)$$

2.2.3 Effective Dose (ED):

The total of weighted equivalent doses, which weighted by a factor referred to as the "tissues weighting factor" (W_T) to reflect the organ or tissue's contribution to the total radiation drawback due to stochastic impact, is used to determine the whole-body dose and the possibility of possible long-term consequences (stochastic effects)(Antoni and Bourgois 2017).

$E\ (Sv) = \sum W_T H_T$ ..... (2)

2.2.4 CT Dose Index (CTDI):

The CT dose index (measured in mGy) is a standardized method of comparing the radiation dose performance of different CT scanners that indicates the radiation output of the scanner. Historically, $CTDI_{100}$ (measured over a 100 mm long ionization chamber) and $CTDI_w$ (weighted average of dose over a single slice) were used however, the more widely used index is $CTDI_{vol}$, which is calculated by dividing $CTDI_w$ by the pitch factor.

2.2.5 Dose Length Product (DLP):

As $CTDI_{vol}$ doesn't take the scan length into account, a new dose index developed by combining the scan length and the $CTDI_{vol}$ resulted in dose length product (DLP) measured in mGy.cm

2.3. Previous Studies

2.3.1 Risk from Ionizing Radiation:

Tepper et al. (2008) reviewed the basics of CT scanning and concentrated on the rising frequency of CT scans acquired, the accompanying radiation doses and the resulting cancer risks in individuals, especially children, they concluded that ionizing radiation, such as x-rays, is uniquely energetic enough to resolve the binding energy of electrons orbiting atoms and molecules, hence, these radiations will knock electrons out of their orbits, resulting in the formation of ions. The most likely situation in biological material exposed to x-rays is the formation of hydroxyl radicals as a result of x-ray interactions with water molecules; these radicals then interact with nearby (DNA), causing strand breaks or base damage. X-rays can also directly ionize DNA. While the majority of radiation-induced damage is rapidly repaired by different cellular systems, DNA double-strand breaks are less quickly repaired, and occasional disrepair can result in the induction of point mutations, chromosomal translocations, and gene fusions, most of which are associated with the development of cancer(Tepper 2008).

In the same study the author concluded that compared to plain-film radiography, CT uses significantly higher doses of radiation, resulting in a significant rise in population radiation exposure. The increase in CT usage and CT-derived radiation dose in the population coincides with a significant improvement in our understanding of the carcinogenic potential of low doses of x-ray radiation. Raman et al. (2013) reviewed eight basic CT scan parameters that may be changed or improved to decrease patient radiation dosage as a result of studies that suggest that up to 0.4 percent of all malignancies in the United States may be attributed to radiation from CT studies conducted between 1991 and 1996 and that radiation from CT studies currently being performed which eventually account for 1.5 percent to 2% of all upcoming cancers(Raman et al. 2013).

In a study (Ionizing Radiation in Medical Imaging and Efforts in Dose Optimization), the authors highlighted that medical radiation is by far the most common artificial source of ionizing radiation exposure, accounting for 90% of all exposures from artificial sources. This radiation burden is becoming more serious. This rise has been attributed largely to the increased use of

computed tomography in the United States (CT). Although CT accounts for just 11% of tests, it accounts for 68% of the total dose. By contrast, traditional radiography accounts for 90% of examinations but accounts for just 19% of the total dose(Vardhanabhuti and A. 2012).

According to the same study, current radiation safety policies and procedures are predicated on the assumption that any amount of radiation, regardless of its magnitude, will cause adverse health effects such as cancer and genetic harm. Additionally, it is believed that these effects are proportional to the dose obtained, i.e., doubling the radiation dose doubles the effect. These two assumptions lead to a dose-response relationship, also referred to as the linear no-threshold model.

Based on the biological effects of ionizing radiation report VII (BEIRVII) Committee, implies that a single population dosage of 10 mSv is associated with a 1 in 1000 lifetime attributable risk for having solid cancer or leukemia. Overall, the probability of developing solid cancer or leukemia from any cause is 42 in 100(BEIR 2006).

In a study titled (Health effects of ionizing radiation from diagnostic CT), referring doctors in the emergency room are overwhelmingly unaware of the risk associated with CT radiation exposure, with only 9% aware of an elevated risk of cancer. Radiation exposure is a minor concern for radiologists performing CT tests, with just 47% aware of the elevated risk of cancer(Martin and Semelka 2006).

Lee et al. (2004) assessed the degree of knowledge among patients, emergency department (ED) physicians, and radiologists regarding radiation dosage and potential hazards associated with computed tomographic (CT) scans, indicated that with increased use comes to a greater awareness of the risks associated with diagnostic CT. Diagnostic CT doses are comparable to those obtained by Japanese atomic bomb survivors, who had a low but statistically relevant dose. For instance, an increased risk of cancer has been reported in long-term survivors of the Hiroshima and Nagasaki atomic bombs who were exposed to 10–100 millisieverts of radiation (mSv).

A single CT scan will expose patients to an equal amount of radiation, and patients can undergo multiple CT scans over time. As a result, there is an increased risk of developing cancer, patients receive little education about the risks, advantages and radiation dose associated with a CT scan.

Regardless of their level of experience, patients, ED doctors, and radiologists are all incapable to offer reliable estimations of CT dosages(Lee et al. 2004).

Based on (CT Evaluation of Diffuse Infiltrative Lung Disease Dose Considerations and Optimal Technique) study, a chest CT examination (3–6 mSv) exposes the patient to 60–120 times the radiation exposure of a posteroanterior chest radiograph obtained on film, the International Commission on Radiological Protection (ICRP) calculated the additional 50 fatal cancers caused per million people exposed to 1 mSv of medical radiation using a linear no-threshold extrapolation of nuclear explosion data(Mayo 2009).

2.3.2 Radiation Doses from Chest HRCT Protocol:

Jang et al. (2016) tracked the long-term variations in CT radiation doses from various CT protocols and to quantify supervising radiologists' long-term efforts to minimize medical radiation. The findings showed that in 2007 the average effective dose of patients who undergrown chest HRCT was 12 ±11.7 mSv, compared to 4.9 ± 3.1 mSv in 2010, different types of scanners were used with a different number of detectors. This substantial reduction in effective dose was achieved as a result of radiologists and the medical community's efforts to optimize the CT scan protocol by modifying parameters in response to clinical demands or unique situations involving certain patients while preserving appropriate image quality(Jang et al. 2016).

Ghetti et al. (2020) assessed the dosimetric effects of high-resolution thorax CT throughout COVID-19 epidemic for 3224 patients in University Hospital of Parma, a low-dose HRCT protocol was used as a result 4.4 mSv was the average effective dose, which ensured low radiation doses and an extremely low-risk assessment(Ghetti et al. 2020a).

2.3.3 Recommended Chest HRCT Protocol During the Pandemic:

Radpour et al. (2020) developed a low-dose high-resolution computed tomography (HRCT) technique for the Iranian Society of Radiology to assess patients with a high risk of COVID-19 infection. The developed protocol was designed to operate with all CT scanners that have four or more detectors and is specific to each manufacturer and mode. The following parameters have been suggested to minimize the radiation dose: Kvp ranges between 100 and 120, mAs ranges between 50 and 100, pitch ranges between 0.8 and 1.5, and thickness ranges between 1-3 mm(Radpour et al. 2020).

Chapter Three

Materials and Methods

This chapter describes the experimental design of the study, from data gathering to successful dose estimates and lifetime cancer risk assessment, as well as statistical analysis and comparison.

3.1 Introduction

This study aimed at investigating the dosimetric impact of high-resolution thorax CT throughout the COVID-19 outbreak at Beit-Jala Governmental Hospital (Al-Hussein), in Bethlehem city. Therefore, organ doses and effective doses were assessed. Then, following the Biological Effects of Ionizing Radiations (BEIR) VII report), we studied the cancer risk associated with these exposures.

3.2 Study Design, and Population

Quantitative retrospective cohort analysis was used to achieve the aim of the study. Between April 26th, 2020, and March 20th, 2021, about 312 (HRCT) of the chests were carried out at Beit-Jala Governmental Hospital (Al-Hussein). The study population of the study consists of 49 adult patients (31 males and 17 females), aged 18 to 89 years who underwent (HRCT) during this period. There were no children found to be considered in this study.

3.3 Exclusion Criteria

- All patients without available anthropometric data such as weight and height.

3.4 Image Acquisition and Reconstruction

The images were acquired using a Philips Brilliance Mx8000 IDT$^{@}$ full power 16-slice CT-scanner (Cleveland, OH). All images were reconstructed using the FBP algorithm. Because of the rapid spread of COVID-19, an already present Thorax HR protocol was used to evaluate patients with diagnosed idiopathic interstitial pneumonia.

was widely used to examine COVID-19-patient. The scan parameters used are mentioned in **Table (3.1)**.

Table 3.1: Fixed scanning parameters used in this study.

Scan Parameters	Setting
Collimation	16*1.5
Slice thickness	3 mm
Increment	-1.5 mm
Scan length	370 mm
Pitch	0.94
Image matrix	512 × 512
Rotation time	0.5 second
kVp	120
Effective mAs	250
Dose modulation	OFF

3.5 Data Collection

Data were collected by using the local picture archiving and communication system (PACS). The DICOM header and CT Radiation Dose Structured Report (RDSR) files produced by the scanner's worksheet were used to extract data from the CT examinations performed. To ensure greater precision and continuity, data was entered into predefined self-designed worksheets as shown in APPENDIX 1, these data include:

- Patient demographic and anthropometric data (age, gender, weight, and height). From the height and weight of each patient, the body mass index was (BMI) also calculated and reported to use as an indicator of body habitus
- Dose descriptive are gathered (CTDIv and DLP).

- **Acquisition length**

Acquisition length was stated in centimeters and was calculated as a shift in position between the initial and final acquisition sections, by the equation(ICRP 92 2003):

$$\text{irradiated lengt} = \text{DLP} \div \text{CTDIvol} \quad (3)$$

3.6 Radiation Dose Calculation

3.6.1 Method 1: Using DLP and k Coefficients from the ICRP 103:

The tissue conversion coefficient (k) for the chest CT was used to calculate the effective dose (ED), expressed in millisieverts (mSv). Which equal 0.014 (mSv mGy-1 cm-1) and dose length product (DLP) in (mGy cm), according to ICRP 10 publication(ICRP 92 2003), by the equation:

$$ED = k \times DLP \quad (4)$$

3.6.2Method2:UsingVirtualDose™CTsoftware:

The estimation of effective dose and organ doses for chest CT scans utilized the (VirtualDoseTM) CT software. This software was employed to assess organ doses and effective doses for both adult and pediatric patients undergoing various computed tomography (CT) examinations, The software is based on an extensive database of organ doses generated through Monte Carlo (MC) simulations using a library of 25 anatomically realistic phantoms expressing people with different ages, body sizes, body weights, and pregnancy stages (Ding et al. 2015)

VirtualDose models several imaging characteristics (energy spectrum, collimation, filtration, and tube current) and clinical protocols using a Monte Carlo-based computational technique. Designers back it up with a comprehensive organ dose database that was established and is still being maintained using Monte Carlo scanner models and the organ-dose and effective-dose algorithms specified in ICRP-60 and ICRP-103.

This software is built as a Software as a Service (SaaS) platform to enable as many users as possible to access it simultaneously via the Internet(Ding et al. 2015). Numerous input parameters are entered through the main interface to calculate organs doses, as shown in (APPENDIX 2), CTDIw (per 100 mAs) or weighted CTDI is an important parameter that indicates the scanner output and is a default value supplied from scanner selection. For accurate calculations, CTDIw (per 100 mAs) will be calculated using the following equation:

$$CTDIw = CTDIvol \; x \; pitch \quad (5)$$

Organ and effective doses were estimated using the VirtualDoseTM CT software, which was based on dose indicators and demographic patient tomography data. Effective dose reflects the overall radiation exposure and is a widely employed physical quantity for comparing doses from different CT scan technologies. Organ doses, on the other hand, are more appropriate indicators of the lifetime risk of induced cancer related to ionizing radiation exposure. Organs considered in this study are Lung, heart, breast, thyroid, liver, kidney, spleen, colon, thymus, red bone marrow, gonads, and stomach. Because of their large surface areas and increased radiosensitivity, these organs are expected to receive high radiation doses during chest CT examinations.

3.7 Cancer Risk Estimation

The lifetime attributable risks (LARs) of cancer induction were estimated from organ equivalent doses using the Biological Effects of Ionizing Radiations (BEIR) VII report. The LAR represents the incidence of solid cancers and of leukemia per 100,000 subjects exposed to a single dose of 0.1 Gy

$$LAR = LAR100 \; (H_T \; / \; 0.1)$$

3.8 Statistical Analysis

Statistical analyses were conducted using Microsoft Excel 2016 and SPSS software, encompassing calculations of mean, median, standard deviation, and 75th percentile values for each dosimetric parameter (CTDIv, CTDIw, DLP, EDMC, and EDDLP). The 75th percentile was employed for comparison with published values, often represented as DRL. Additionally, mean equivalent doses and cancer risk probabilities for organs were determined across gender subpopulations. Spearman's rank-order test assessed correlations between DLP\BMI, EDDLP, and EDMC, with a significance level set at $p < 0.05$.

Furthermore, an independent sample t-test was employed to examine differences in cancer risk probability between genders.

Chapter Four

Results and Discussion

4.1 Results

This chapter summarizes the study's findings, including ED and organ equivalent dose data, as well as the latter's application for cancer risk estimation in the general population and depending on gender and age. including a discussion of the findings, limits, and recommendations.

4.1.1 Study population:

As shown in **Table (4.1)**, the research comprised 48 patients who were examined during the COVID-19 pandemic, with 17 (35.4%) being women and 31 (64.6%) being men. The mean age of our population was 51.3 years (age range 18-89 years), and the mean BMI was 28.4 kg/m^2 (range 18.2-41.8 kg/m^2).

Table 4.1: Presents Demographic Data for The Entire Population as Well as Each Patient's Age-Related Sub-Cohort.

Age category (year)	Female	Male	Total
18-28	0	3	3
29-39	3	4	8
40-50	7	10	17
51-61	2	5	7
>62	5	9	12
Total number/percent	17 (35.4%)	31 (64.6%)	48 (100%)
Mean age	52.2	50.7	51.3
Mean BMI (kg. /m2)	27.4	29	28.44

4.1.2 CT Scan Parameters:

All patients were examined with constant scan parameters except the scan length which varied considerably among them. The mean scan length in both genders is 38.5 cm (range 25.8 - 50). This implies that there is no restriction to the field of view.

4.1.3 Dosimetric Data:

Table (4.2) shows the results of a statistical analysis of CT scan dosimetric parameters as a function of mean value, median, standard deviation, and 75th percentile for the entire population, females, and males.

Table 4.2: Radiation Dose Descriptive

Total	**Mean**	**Median**	**Standard deviation**	**75th**
$CTDI_V$ (mGy)	17.8	17.6	2	18.2
$CTDI_W$	12.6	12.1	2.76	17.1
DLP (mGy.cm	689.59	687.13	121.46	728.9
Female	**Mean**	**Median**	**Standard deviation**	**75th**
$CTDI_V$ (mGy)	18.15	17.6	2.3	17.6
$CTDI_W$	17	16.5	2.169	16.5
DLP (mGy.com)	704.3	666.01	147.99	741.1
Male	**Mean**	**Median**	**Standard deviation**	**75th**
$CTDI_V$ (mGy)	17.7	17.6	1.8	18.2
Total	**Mean**	**Median**	**Standard deviation**	**75th**
$CTDI_W$	16.6	16.5	1.7	17.1
DLP (mGy.cm)	681.1	694.2	104.8	728.9

The mean value of $CTDI_v$ (mGy), $CTDI_w$ (mGy), and DLP (mGy.cm) for the total population are 17.8, 12.6, 689.59 respectively, while the same value for the three-dose descriptive is slightly higher in females than in males.

4.1.4 Effective Dose:

4.1.4.1 Method One: ED_{DLP}

The results of effective dose based on DLP and k factors for the total population, females, and males are presented in **Table (4.3)**. The mean effective dose for the total population is 9.7 mSv ranged from (6.5) to (15.2) mSv, while for females and males are 10 mSv and 9.5 mSv respectively. The highest calculated ED value was 15.22 mSv, belongs to females aged 32 years. Whilst the lowest value achieved calculated is 6.5 mSv belong to a male whose 47-year-old.

Table 4.3: Effective Dose by DLP and k factors.

ED_{DLP} (mSv)	Mean	Median	Standard Deviation	75th
Total population	9.7	9.6	0.24	10.22
Female	10	9.5	2.1	14.25
Male	9.5	9.7	1.5	10.2

4.1.4.2 Method Two: ED_{MC}

The results of effective dose based on Monte Carlo simulation for the total population, females, and males are presented in **Table (4.4).**

Table 4.4: Effective Dose by VirtualDose™ CT software

ED_{MC} (mSv)	Mean	Median	Standard Deviation	75th
Total population	13.47	12.94	2.94	14.93
Female	14.75	13.56	3.57	16.38
Male	12.7	12.8	2.2	14.09

The average effective dose for the total population is 13.47 mSv ranged from (8.51) to (23.17) mSv. While based on gender the female's mean effective doses were higher than that of the males by a factor of (1.2). In simulated ED the highest value is 23.17 mSv, belong to a female who is 32 years old. While the lowest value is 8.5 mSv, belong to a male whose 61 years old.

4.1.4.3 Comparison of Effective Dose Calculation Methods:

The average values of the ED calculated by the two methods are shown in **Fig. (4.1)**. The average value of ED_{DLP} is 9.7 mSv compared to ED_{MC} with an average value of 13.47 mSv, which is higher than the former mean value by a factor of 1.4.

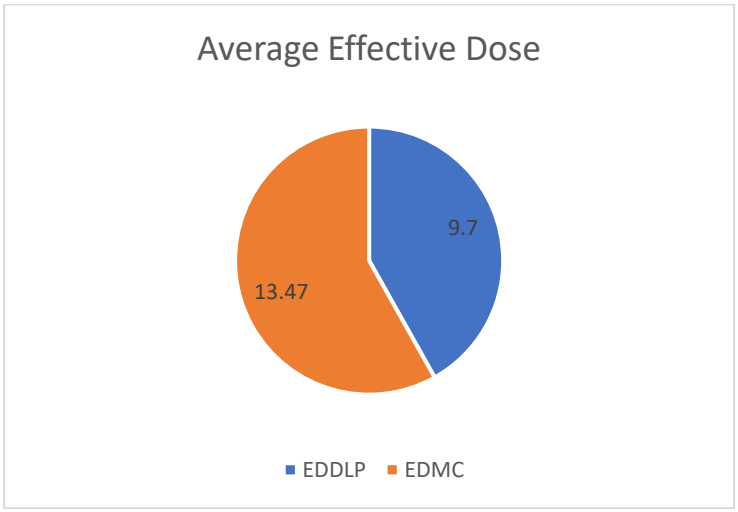

Figure 4.1: Comparison of Effective Dose for ED_{DLP}, ED_{MC}

4.1.4.4 Effective Dose (ED_{MC}) as a Function of Patient BMI and DLP:

The relationship between radiation effective dose and patient BMI and DLP was investigated in this study. **Fig. (4.2)** represents the relationship between radiation effective dose and patient BMI, **Fig. (4.3)** shows the correlation between effective dose and DLP. A linear regression model, and P-value was used to determine the statistical significance of the two relationships.

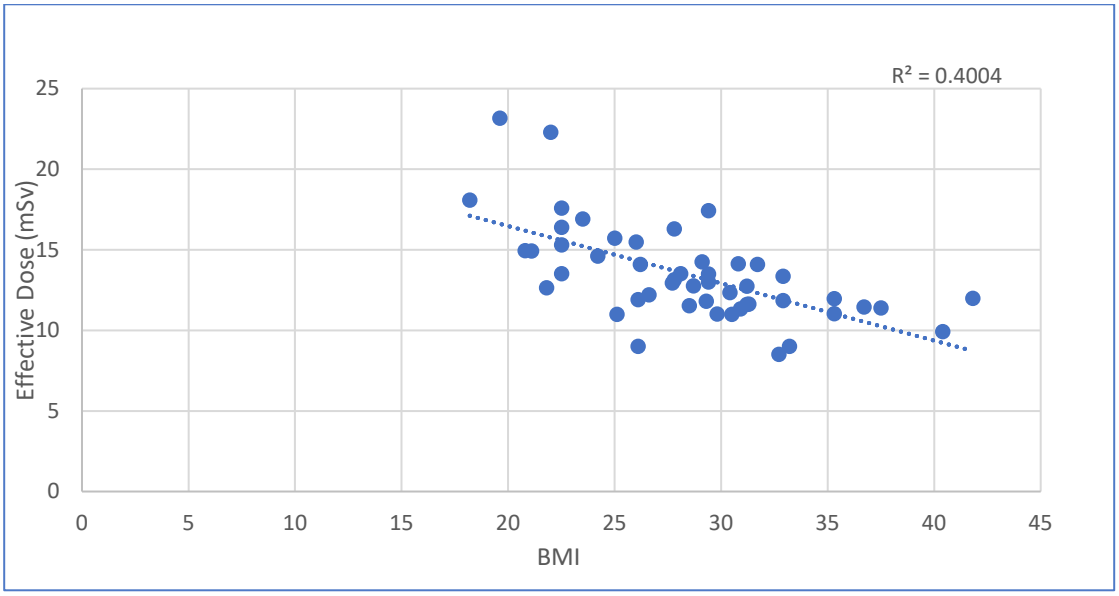

Figure 4.2: Effective Dose (ED_{MC}) as a Function of BMI.

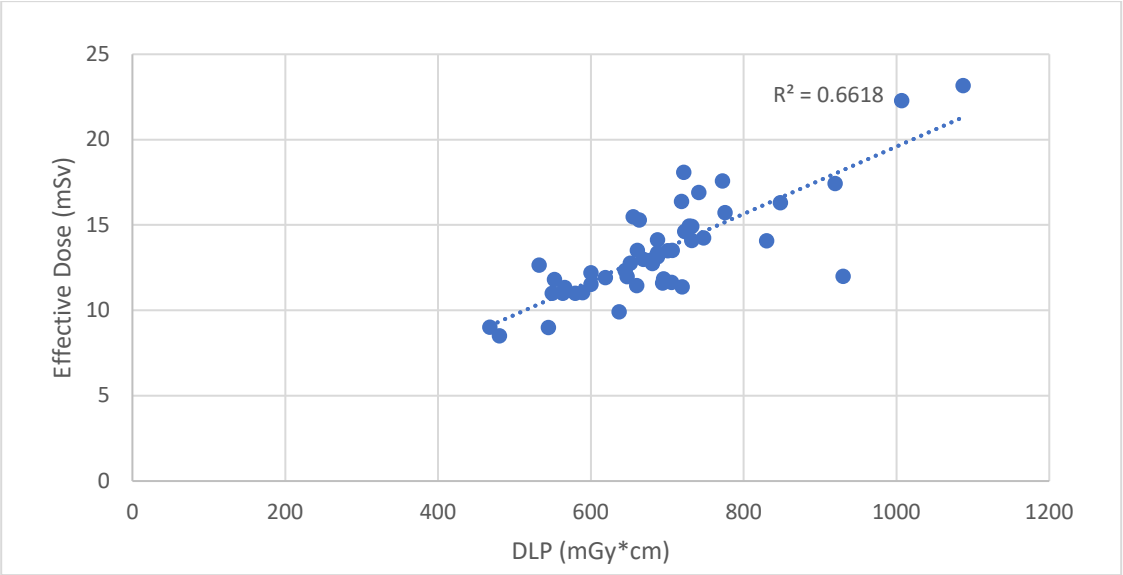

Figure 4.3: Effective Dose (ED_{MC}) as a Function of DLP

4.1.4.5 Effective Dose (ED_{DLP}) as a Function of Patient BMI and DLP:

Fig. (4.4) and Fig. (4.5) demonstrate ED_{DLP} correlations with BMI and DLP respectively.

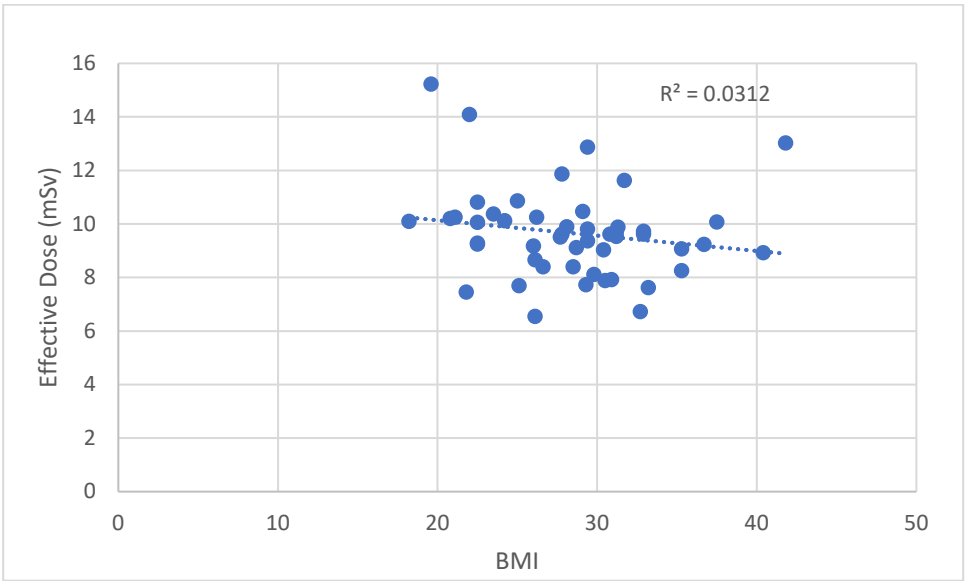

Figure 4.4: Effective Dose (ED_{DLP}) as a Function of BMI.

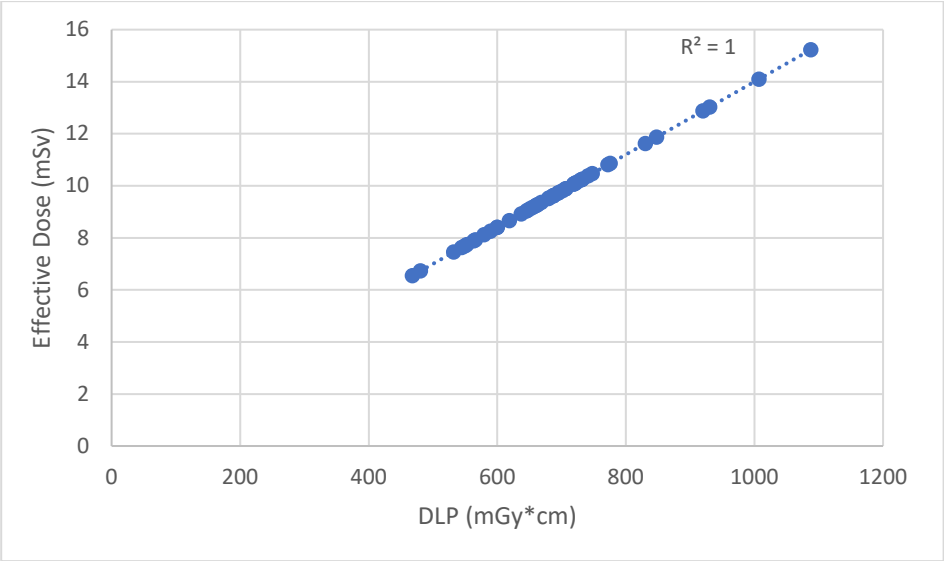

Figure 4.5: Effective Dose (EDDLP) as a function of DLP.

4.1.5 Organ Equivalent Doses:

The average equivalent doses to different organs for both genders are summarized in **Fig. (4.6)** and **Fig. (4.7)**, respectively.

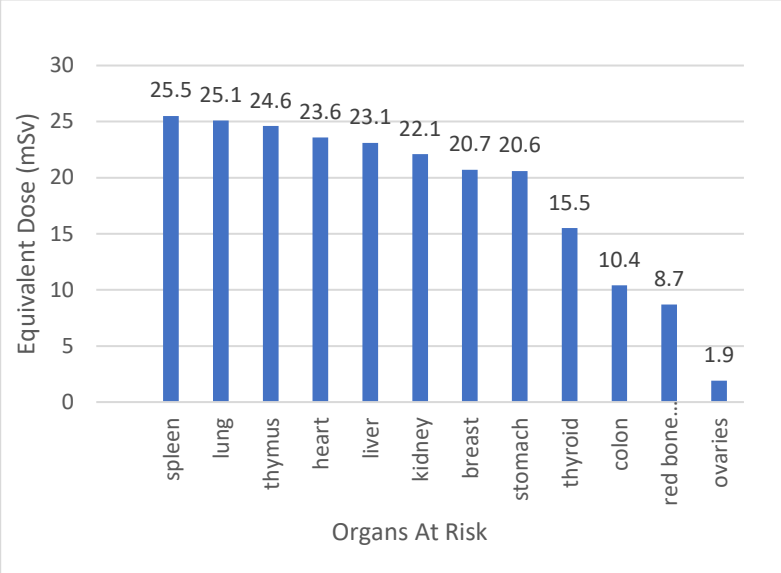

Figure 4.6: Mean organ equivalent dose for females.

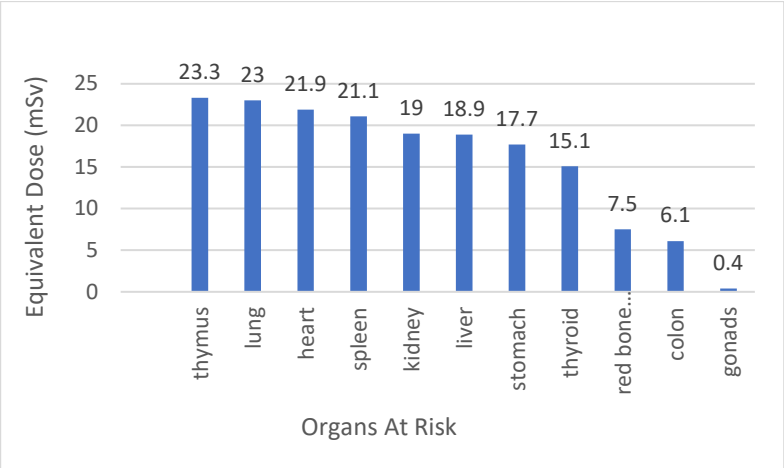

Figure 4.7: Mean organ equivalent dose for males.

The equivalent dose for all organs is higher in females than in males by a factor ranging between 1 and 4.8 based on the organ. In females the highest organ dose found in the spleen with a mean value of 25.5 mSv ranged from 16.5 to 40.7 mSv belong to 80- and 49-years old females respectively. While in males, the thymus gland has the highest dose with a mean value of 23.3 mSv ranged between 15.4 and 31.31 mSv belong to 47- and 61-years old males respectively. The second-highest dose found in lungs in both genders with a mean value of 25.1 and 23 mSv for females and males respectively, the ovaries in females and gonads in males have the lowest dose with an average value of 1.9 and 0.4 mSv respectively.

4.1.6 Cancer Risk:

4.1.6.1 Cancer Risk Probability per Gender:

The **Fig. (4.8)** highlights the average cancer risk per 100,000 individuals for males and females across various cancer types. Among females, lung cancer poses the highest risk (51.6 per 100.000), followed by breast cancer (20 per 100.000), while thyroid cancer has the lowest risk (1.64 per 100.000). For males, lung cancer also ranks highest (21.8 per 100.000), with colon and stomach cancers at moderate levels (6.8 and 4.2, per 100.000 respectively), and thyroid cancer showing the lowest risk (0.5 per 100.000). Overall, lung cancer is the most prevalent for both genders, with females having a significantly higher risk than males, while thyroid cancer consistently poses the least risk.

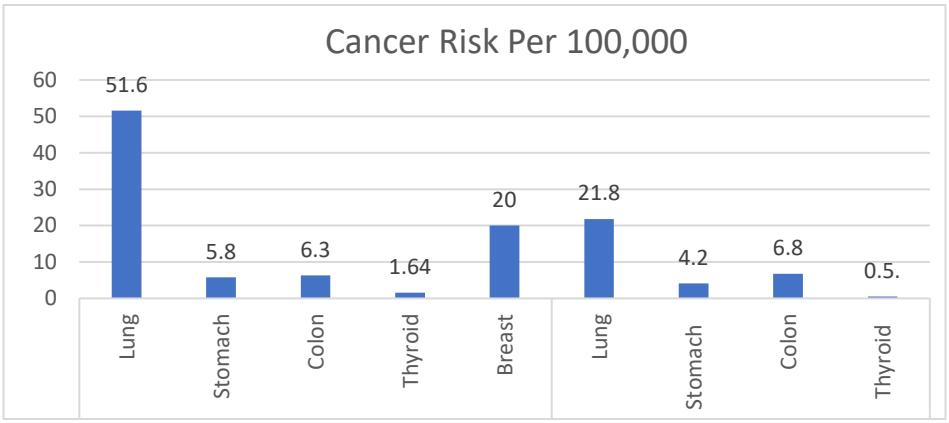

Figure 4.8: the average cancer risk per 10^5 patients in both genders

4.1.6.2 Cancer Risk Per Age for Both Genders:

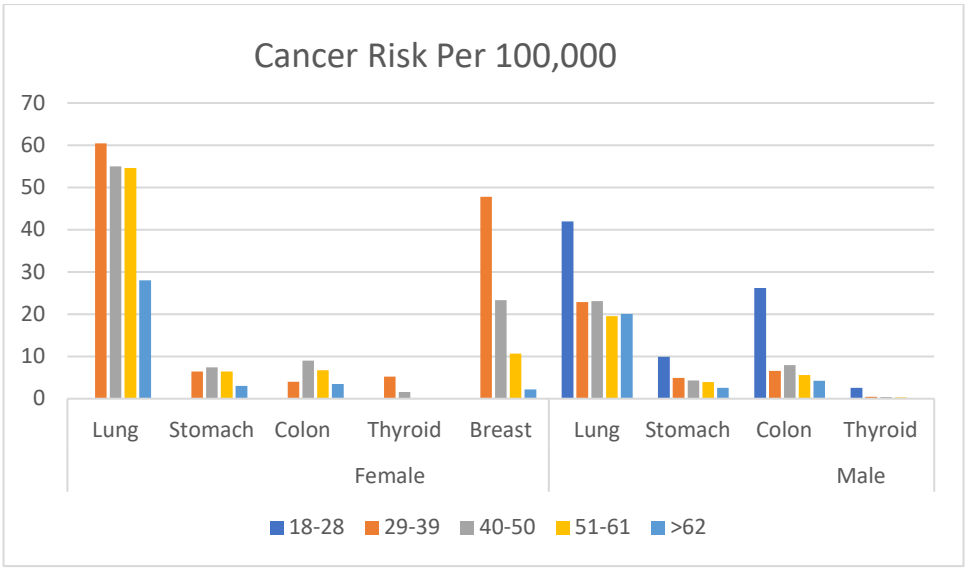

Figure 4.9: Cancer Risk Per age and Gender.

- Cancer risk probabilities varied across ages, as it observed in female lung cancer rates are notably high in the 29-39 age group but decrease with age.
- Male cancer rates, especially for lung and colon cancers, are highest in the younger age groups (18-28).
- Both genders show a significant decrease in rates for cancers like thyroid and stomach cancer as age increases.

This summary highlights age and gender-related trends in cancer risk for each type, with younger individuals generally showing higher rates in most cases. It's important to notice that all age categories include different numbers of patients.

4.1.7 Comparison of our Results with Literature:

4.1.7.1 Dosimetric Data:

The mean value of our dosimetric statistics for CTDIv and DLP for chest HRCT is significantly higher than those published in literature by factors range between 2.3 to 5.3 for $CTDI_v$ and factors ranging from 2.6 to 9.3 for DLP.
The average of CTDIv and DLP values for our study and international studies are summarized in **Table (4.5)**.

Table.4.5 Comparison of the mean of $CTDI_v$ and DLP of the Present Study as Well as other International Drls.

Study	Mean CTDIv	Mean DLP
Present study	18.2	728.9
UK 2003[37]	7	170
Norway 2008[38]	3.4	78
Irland 2010[39]	6.6	276
Iran 2019[40]	7.8	217

4.1.7.2 Effective Dose:

Table (4.6) compared the effective dose of the present study with other international studies, as it shows the mean value of the effective dose of the present study significantly higher than those of other international studies.

Table 4.6: Comparison of present effective dose with international studies.

Study	Average Effective dose (mSv)
Present study	14.93
Palestine2017(Lahham et al.2018)	7
Sudan 2018(Ismail 2015)	5.43
Italy 2020(Ghetti et al. 2020b)	4.4

4.1.7.3 Cancer Risk:

Table (4.7) shows the cancer risk probabilities of our study compared to similar Italian study, which indicates a significant difference in lung cancer risk in women and men with our values higher than the Italian study, while in stomach there is no significant differences found with our value slightly higher in females and lower value in males.

Table 4.7: Comparison of Present Caner Risk with International Study.

Cancer risk per 10^5	Present study		Italian study	
Organ	Female	Male	Female	Male
Lung	51.6	21.8	25	10
Stomach	5.8	4.2	5	6
Breast	20	-	25	-

4.2 Discussion

4.2.1 Acquisition length:

As mentioned earlier , the scan length in this study varied across patients ranged from (25.8 to 50)cm, the highest value indicates an extremely large FOV that extended from orbital margins superiorly to the abdomen, beyond the typical chest limits that can be extended up to 35 cm extends from the lung apices to the costophrenic sulci(ACR.2020).For example, two males with same weight and high (85-160) the effective dose increased from (9 to 11.6) mSv as the scan length increased from (30.9 to 35.9) cm. In this research, it was observed that rising radiation dosage corresponded to expanding field of view, which is consistent with literature that concluded as the scan length is increased, the dosage increases linearly(Rawashdeh et al. 2021)

4.2.2 Dosimetric Data:

Our dosimetric data in terms of $CTDI_{VOL}$ and DLP stated in the mean value for chest HRCT are substantially greater than those reported in the literature, with factors range between 2.3 to 5.3 for $CTDI_{VOL}$, and factors ranging from 2.6 to 9.3 for DLP.

These differences between our study and other studies are attributed to the differences between the scanners and scan parameters used. For example, the $CTDI_{VOL}$ and DLP values reported in Iran (2019) are high compared to values levels published in literature, even though they are lower than our values by a factor of 2.3 and 3.3 respectively, such differences can be explained by the different parameters used which are listed in **Table (4.8)**. All parameters are expressed in mean value.

Table 4.8: The Average Value of Scan Parameters of Present Study and Another International Study.

Study	Kvp	mAs	Scan length(cm)	Rotation time(s)	Slice thickness(mm)
Present	120	250	38.5	0.5	1.5
Iran 2019	121	152	27.54	0.62	0.82

However, these significant distinctions indicate that the protocol parameters used in this study has to be optimized.

4.2.3 Effective Dose:

4.2.3.1 ED_{DLP}:

The calculated effective dose higher in females than in males with no significant difference observed, this slight difference could be due to the small difference in DLP between both gender, which is higher in females than males. The highest calculated effective dose was 15.22 mSv which belong to 32 years old female associated with the highest acquisition length of 50 cm and highest DLP value of 1087.35 mGy*cm, while the lowest calculated value was 6.5 mSv belong to 47 years old male associated with the lowest DLP value of 467.84 mGy*cm.
Calculated effective dose variation was highly depending on DLP with a correlation factor (R^2) equal 1, on the other hand there was no observed relationship between calculated effective dose and patient BMI with (R^2) equal 0.03

4.2.3.2 ED_{MC}:

The mean effective dose in females higher than in males by a factor of 1.2, this is explained by the fact that radiosensitivity higher in females which has been reported in important human researches on the health effects of radiation exposure(Narendran et al. 2019). 23.17 mSv is the highest simulated effective dose which belong to a 32 years old female has a BMI of 19.6 kg. /m2 associated with the highest scan length and DLP values of 50 cm and 1087 mGy*cm respectively, the lowest effective dose value was 8.5 mSv belong to an adult male aged 61 years, associated with the lowest acquisition length and DLP values of 25.8 cm and 480.53 mGy*cm and has a BMI value of 32.7 kg. /m2.these data urged us to investigate the correlation between effective dose with BMI and DLP, as a result it was found a moderate negative relationship between effective dose and BMI with ($R^{\wedge 2}$) equal 0.40 and a P-value of 0.000006 which indicated a highly significant correlation, in other words 40% of the effective dose variation depending on BMI variation, this negative correlation shows that patients with greater BMI received lower radiation doses, which might be explained by the adipose tissue acting as a radiation shield for the internal organs, and this conclusion was consistent with other researches as (DeMarco et al. 2007; Ding et al. 2015; Liang et al. 2017).

Regarding DLP it was found a stronger positive correlation with effective dose with ($R^{\wedge 2}$) = 0.66 and a P-value = 0.000000000001, which means 66% of the effective dose variation could be explained by the DLP variation.

4.2.3.3 Comparison of Effective Dose Calculation Methods:

As proven earlier the average ED_{MC} (13.47) mSv higher than the average of ED_{DLP} (9.7) mSv by a factor of 1.4, this is due to the fact that particular patient features Underrepresented by the conventional method of effective dose calculation(Kopp et al. 2020).

4.2.4 Organ Equivalent Doses:

Females have higher organ equivalent doses for all organs than those for males this indicates a higher radiosensitivity in females than males, this results comparable with other available researches, for example, a Canadian study published in 2019 which assessed significant human studies on the health concerns associated with radiation exposure concluded that women have higher long-term radiosensitivity than males who absorb a comparable dosage of radiation. According to the same research the National Academy of Sciences' study on the biological effects of ionizing radiation (BEIR VII), published in 2006 emphasized that women may be at much greater risk of harm and death from radiation-induced cancer than males who have received the same dosage of radiation.(Narendran et al. 2019)

Spleen (in females) and thymus (in males) have the greatest dosages among other organs, which may be attributed to the fact that these organs belong to the hematopoietic system, which has a greater sensitivity compared to other systems due to their higher active cell division (IAEA3), the lung has the second highest dose in both gender with no significant differences as the doses are 25.5 and 23.3 (mSv) for females and males respectively, gonads equivalent doses in both gender were the lowest this is as a result of the distal location of these organs from the primary field of view, despite the result that female gonads absorbed higher radiation dose than males gonads by a factor of 4, this indicates the higher radiosensitivity of female gonads.

4.2.5 Cancer Risk:

4.2.5.1 Cancer Risk Probability per Gender:

To assess the effects of radiation exposure associated with these diagnostic tests for both genders, the average cancer risk for the lung, stomach, colon, thyroid, and breast per 100,000 patients is determined. As expected, lung cancer was the primary condition that could be caused by diagnostic exposures in both genders, and it was more frequent for women than men by a factor of 2.3. In females, the breast cancer is the second health complication that could happened with a risk value of 20 per 100.000, which explained by the high radiosensitivity of the mammary gland in female breast, on the other hand the colon cancer was the second highest condition in males with a risk value of 6.8 per 100.000 which is slightly higher than in females.

Overall, the cancer risk for all types is higher in females than males except for colon cancer risk, this indicates a higher radiosensitivity for females with significant differences for lung and stomach cancer, the lung and stomach risk differences were in favor of the female participants (MV 51.6, MV 5.8) compared to (MV 21.8, MV 4.5) for the male patients as shown in **Table (4.9).**

Table 4.9: Cancer Risk Estimation Per Gender.

Organ	gender	N	Mean	Std. Deviation	P-Value	
stomach	male	31	4.2	2.09	0.040	significant
	female	17	5.8	2.63		
colon	male	31	6.8	6.92	0.750	Not significant
	female	17	6.3	3.9		
lung	male	31	21.8	7.9	6.86×10^{-6}	significant
	female	17	51.6	19.19		
thyroid	male	31	0.5	0.8	0.131	Not significant
	female	17	1.6	2.8		
breast	male	0			-	-
	female	18	23.24	3.95		

However , these outcomes are comparable with literature in which a published study in 2019 reviewed considerable studies on the effects of radiation exposure on health, which concluded that after Chernobyl accident the incidence of cancer and mortality was 50% greater in women than in men after receiving the same radiation dose, even though both men and women had numerous radiation-related health issues, women's reproductive capacities were negatively impacted by the consequences, which appeared to be more pronounced in women, according to the same review atomic bomb survivors from Hiroshima and Nagasaki have showed elevated risks for solid tumors that differ by gender, and solid cancer rates rise by approximately 35% per Gy for men and 58% per Gy for women in adults aged 70 who were exposed to radiation at the age of 30. (Narendran, et al. 2019).

- Stomach and lung cancer show statistically significant differences between genders, with females having higher risks.
- Colon and thyroid cancer differences are not statistically significant

4.2.6 Comparison of our Results with Literature:

4.2.6.1 Dosimetric Data and Effective Dose:

The dosimetric data of our study in terms of $CTDI_v$ and DLP were substantially higher compared to those typically reported in literature by factors range between 2.3 to 5.3 and 2.6 to 9.3 for

CTDIv and DLP respectively, moreover the mean value of our effective dose was higher than other reposted in literature by a factor ranging from 2.2 to 2.9.

This variation could be explained by two main reasons. Firstly, the scan length, as mentioned earlier there was no restriction on the length of the scan. Secondly, the tube current-time product (mAs) was not utilized for each patient, despite the fact that the automatic exposure control (AEC) system is applied to reduce patient exposure, a constant mAs parameter was used for all patients instead. It needs to be stated that variations in effective dose may also exist related to population demography and calculation method as well. In conclusion these variations point to the need to optimize our imaging protocol in order to reduce patient dose.

4.2.6.2 Cancer Risk:

When compared our findings to those of an Italian study that investigated the dosimetric impact of a chest HRCT scan during COVID-19, our result showed a higher cancer risk in all organs with a significant difference in lung cancer risk for both genders, this significant difference could be attributed to the different protocol employed, which used a low dose protocol that activated the CARE Dose 4D AEC using effective 110 mAs.

Chapter Five

Conclusions Recommendations and Limitations

5.1 Conclusion

The current chest HRCT protocol has higher Dosimetric data in terms of CTDIV and DLP than reported in literature. In addition to radiation effective dose and cancer risk values.
Females showed a higher organs dose than males for all organs in addition to the effective dose and cancer risk except for colon cancer. Compared to previous studies, the data revealed that women are more prone to experiencing cancer than men in some organs. The primary cancer risk found in lungs for both genders.

5.2 Recommendations

1- The current HRCT protocol parameters must be optimized.
2- Patient age and weight should be taken into account.

5.3 Limitations

1- Sample size was limited due to lack of patient information needed for research.
2- Bias.

References

Alam, Syed Zoherul, SMA Al Muid, Afroza Akhter, AKM Sharifur Rahman, Md Al Emran, and Md Tarif Al Mostakim. 2020. 'HRCT Chest Evaluation of COVID-19 Patients: Experience in Combined Military Hospital Dhaka, Bangladesh'. *Journal of Bangladesh College of Physicians and Surgeons*, June, 21–28. https://doi.org/10.3329/jbcps.v38i0.47441.

Antoni, Rodolphe, and Laurent Bourgois. 2017. *Applied Physics of External Radiation Exposure*. https://doi.org/10.1007/978-3-319-48660-4.

BEIR. 2006. *Health Risks from Exposure to Low Levels of Ionizing Radiation: BEIR VII Phase 2*. *Health Risks from Exposure to Low Levels of Ionizing Radiation: BEIR VII Phase 2*. https://doi.org/10.17226/11340.

Berrington De González, Amy, Mahadevappa Mahesh, Kwang Pyo Kim, Mythreyi Bhargavan, Rebecca Lewis, Fred Mettler, and Charles Land. 2009. 'Projected Cancer Risks from Computed Tomographic Scans Performed in the United States in 2007'. *Archives of Internal Medicine* 169 (22): 2071–77. https://doi.org/10.1001/archinternmed.2009.440.

Cantatore, Angela, and Pavel Müller. 2011. 'Introduction to Computed Tomography'.

Corcoran, Helen L, William R Renner, and Michaelj Milstein. n.d. 'Resolution CT-; Ofthe Lung1'.

DeMarco, J. J., C. H. Cagnon, D. D. Cody, D. M. Stevens, C. H. McCollough, M. Zankl, E. Angel, and M. F. McNitt-Gray. 2007. '2007'. *Physics in Medicine and Biology* 52 (9): 2583–97. https://doi.org/10.1088/0031-9155/52/9/017.

Ding, Aiping, Yiming Gao, Haikuan Liu, Peter F. Caracappa, Daniel J. Long, Wesley E. Bolch, Bob Liu, and X. George Xu. 2015. 'VirtualDose: A Software for Reporting Organ Doses from CT for Adult and Pediatric Patients'. *Physics in Medicine and Biology* 60 (14): 5601–25. https://doi.org/10.1088/0031-9155/60/14/5601.

Elicker, Brett M., Kimberly G. Kallianos, and Travis S. Henry. 2017. 'The Role of High-Resolution Computed Tomography in the Follow-up of Diffuse Lung Disease'. *European Respiratory Review* 26 (144). https://doi.org/10.1183/16000617.0008-2017.

Finance, Julie, Laurent Zieleskewicz, Paul Habert, Alexis Jacquier, Philippe Parola, Alain Boussuges, Fabienne Bregeon, and Carole Eldin. 2021. ‘Low Dose Chest CT and Lung Ultrasound for the Diagnosis and Management of COVID-19’. *Journal of Clinical Medicine* 10 (10): 2196. https://doi.org/10.3390/jcm10102196.

Foley, Shane J., M. F. Mcentee, and L. A. Rainford. 2012. ‘Establishment of CT Diagnostic Reference Levels in Ireland’. *British Journal of Radiology* 85 (1018): 1390–97. https://doi.org/10.1259/bjr/15839549.

Friberg, Eva Godske, Anders Widmark, Ingrid Helen, Ryste Hauge, Norwegian Radiation, Protection Authority, P O Box, and N- Østerås. 2009. ‘National Collection of Local Diagnostic Reference Levels in Norway and Their Role in Optimization of X-Ray Examinations’. *Norwegian Radiation Protection Authority*, no. 1, 1–10. http://www.nrpa.no/publikasjoner.

Ghetti, C., O. Ortenzia, M. Maddalo, L. Altabella, and N. Sverzellati. 2020a. ‘Dosimetric and Radiation Cancer Risk Evaluation of High-Resolution Thorax CT during COVID-19 Outbreak’. *Physica Medica* 80 (December):119–24. https://doi.org/10.1016/j.ejmp.2020.10.018.

———. 2020b. ‘Dosimetric and Radiation Cancer Risk Evaluation of High-Resolution Thorax CT during COVID-19 Outbreak’. *Physica Medica* 80 (May): 119–24. https://doi.org/10.1016/j.ejmp.2020.10.018.

G.Marchal • T.J.Vogl • J.P.Heiken • G.D.Rubin. 2005. ‘Multidetector-Row Computed Tomography Scanning and Contrast Protocols’.

ICRP 92. 2003. *Annals of the ICRP Annals of the ICRP Annals of the ICRP. ICRP Publication 92, Annals of ICRP 28.*

Ismail. 2015. ‘مـــسب الله نمحرلا ميحرلا Sudan University of Science and Technology College of Graduate Studies’, no. September, 1–88.

Jang, Jinhee, Seung Eun Jung, Woo Kyoung Jeong, Yeon Soo Lim, Joon Il Choi, Michael Yong Park, Yongsoo Kim, et al. 2016. ‘Radiation Doses of Various CT Protocols: A Multicenter Longitudinal Observation Study’. *Journal of Korean Medical Science* 31:S24–31. https://doi.org/10.3346/jkms.2016.31.S1.S24.

‘Jcpsp_2008_18_6_327_328’. n.d.

Kopp, Markus, Tobias Loewe, Wolfgang Wuest, Michael Brand, Matthias Wetzl, Wolfram Nitsch, Daniela Schmidt, et al. 2020. ‘Individual Calculation of Effective Dose and Risk of Malignancy Based on Monte Carlo Simulations after Whole Body Computed Tomography’. *Scientific Reports* 10 (1): 1–12. https://doi.org/10.1038/s41598-020-66366-2.

Lahham, Adnan, Hussein ALMasri, and Saleh Kameel. 2018. ‘Estimation of Female Radiation Doses and Breast Cancer Risk from Chest CT Examinations’. *Radiation Protection Dosimetry* 179 (4): 303–9. https://doi.org/10.1093/rpd/ncx283.

Lee, Christoph I., Andrew H. Haims, Edward P. Monico, James A. Brink, and Howard P. Forman. 2004. ‘Diagnostic CT scans: Assessment of Patient, Physician, and Radiologist Awareness of Radiation Dose and Possible Risks’. *Radiology* 231 (2): 393–98. https://doi.org/10.1148/radiol.2312030767.

Liang, Baohui, Yiming Gao, Zhi Chen, and X. George Xu. 2017. ‘Evaluation of Effective Dose from Ct Scans for Overweight and Obese Adult Patients Using the Virtualdose Software’. *Radiation Protection Dosimetry* 174 (2): 216–25. https://doi.org/10.1093/rpd/ncw119.

Martin, Diego R., and Richard C. Semelka. 2006. ‘Health Effects of Ionising Radiation from Diagnostic CT’. *Lancet* 367 (9524): 1712–14. https://doi.org/10.1016/S0140-6736(06)68748-5.

Mayo, John R. 2009. ‘CT Evaluation of Diffuse Infiltrative Lung Disease: Dose Considerations and Optimal Technique’. *Journal of Thoracic Imaging* 24 (4): 252–59. https://doi.org/10.1097/RTI.0b013e3181c227b2.

METER, WORLD. 2021. ‘Https://Www.Worldometers.Info/Coronavirus/’.

Narendran, Nadia, Lidia Luzhna, and Olga Kovalchuk. 2019. ‘Sex Difference of Radiation Response in Occupational and Accidental Exposure’. *Frontiers in Genetics* 10 (MAY): 1–11. https://doi.org/10.3389/fgene.2019.00260.

Padley, ^, F Gleeson, and C D R Flower. 1995. ‘The British Journal of Radiology Review Article: Current Indications for High Resolution Computed Tomography Scanning of the Lungs’. *The British Journal of Radiology*. Vol. 68.

Radpour, Alireza, Hooman Bahrami-Motlagh, Mohammad Taghi Taaghi, Abdolrasul Sedaghat, Mohammad Ali Karimi, Ali Hekmatnia, Hamid Reza Haghighatkhah, Morteza Sanei-Taheri, Mehran Arab-Ahmadi, and Arash Azhideh. 2020. 'COVID-19 Evaluation by Low-Dose High Resolution CT Scans Protocol'. *Academic Radiology* 27 (6): 901. https://doi.org/10.1016/j.acra.2020.04.016.

Raman, Siva P., Mahadevappa Mahesh, Robert V. Blasko, and Elliot K. Fishman. 2013. 'CT Scan Parameters and Radiation Dose: Practical Advice for Radiologists'. *Journal of the American College of Radiology* 10 (11): 840–46. https://doi.org/10.1016/j.jacr.2013.05.032.

Rawashdeh, Mohammad Ahmmad, and Charbel Saade. 2021. 'Radiation Dose Reduction Considerations and Imaging Patterns of Ground Glass Opacities in Coronavirus: Risk of over Exposure in Computed Tomography'. *Radiologia Medica* 126 (3): 380–87. https://doi.org/10.1007/s11547-020-01271-2.

Revel, Marie Pierre, Anagha P. Parkar, Helmut Prosch, Mario Silva, Nicola Sverzellati, Fergus Gleeson, and Adrian Brady. 2020. 'COVID-19 Patients and the Radiology Department – Advice from the European Society of Radiology (ESR) and the European Society of Thoracic Imaging (ESTI)'. *European Radiology* 30 (9): 4903–9. https://doi.org/10.1007/s00330-020-06865-y.

ROMANS, LOISE E. 2011. 'Computed Tomography for Technologists A Comprehensive Text by Lois Romans (z-Lib.Org)'.

Schoepf, U. J., R. D. Bruening, C. Hong, R. Eibel, S. Aydemir, A. Crispin, C. Becker, and M. F. Reiser. 2001. 'Multislice Helical CT of Focal and Diffuse Lung Disease: Comprehensive Diagnosis with Reconstruction of Contiguous and High-Resolution CT Sections from a Single Thin-Collimation Scan'. *American Journal of Roentgenology* 177 (1): 179–84. https://doi.org/10.2214/ajr.177.1.1770179.

Shrimpton, Paul C., M. C. Hillier, M. A. Lewis, and M. Dunn. 2006. 'National Survey of Doses from CT in the UK: 2003'. *British Journal of Radiology* 79 (948): 968–80. https://doi.org/10.1259/bjr/93277434.

Singhal, Tanu. 2020. 'A Review of Coronavirus Disease-2019 (COVID-19)'. *Indian Journal of Pediatrics*. Springer. https://doi.org/10.1007/s12098-020-03263-6.

Tepper, Stewart J. 2008. 'Computed Tomography - An Increasing Source of Radiation Exposure: CommentaryTepper, S. J. (2008). Computed Tomography - An Increasing Source of Radiation Exposure: Commentary. Headache, 48(4), 657. Https://Doi.Org/10.1111/j.1526-4610.2008.01071.x'. *Headache* 48 (4): 657. https://doi.org/10.1111/j.1526-4610.2008.01071.x.

This, Preamble, Practice Parameters, and Technical Standards. 2020. 'Acr – Str Practice Parameter for the Performance of High- Resolution Computed Tomography (Hrct) of the Lungs in Adults' 1076:1–9.

Tofighi, Salar, Saeideh Najafi, Sean K. Johnston, and Ali Gholamrezanezhad. 2020. 'Low-Dose CT in COVID-19 Outbreak: Radiation Safety, Image Wisely, and Image Gently Pledge'. *Emergency Radiology* 27 (6): 601–5. https://doi.org/10.1007/s10140-020-01784-3.

Vardhanabhuti, Varut, and Carl A. 2012. 'Ionizing Radiation in Medical Imaging and Efforts in Dose Optimization'. *Current Topics in Ionizing Radiation Research*, no. 160. https://doi.org/10.5772/33446.

WHO. 2023. 'Https://Www.Who.Int/Emergencies/Diseases/Novel-Coronavirus-2019/Question-and-Answers-Hub/q-a-Detail/Coronavirus-Disease-Covid-19'.

Wolters, Kluwer. 2014. 'Technical Aspects of High-Resolution CT'.

Yanagawa, Masahiro, Akinori Hata, Osamu Honda, Noriko Kikuchi, Tomo Miyata, Ayumi Uranishi, Shinsuke Tsukagoshi, and Noriyuki Tomiyama. 2018. 'Subjective and Objective Comparisons of Image Quality between Ultra-High-Resolution CT and Conventional Area Detector CT in Phantoms and Cadaveric Human Lungs'. *European Radiology* 28 (12): 5060–68. https://doi.org/10.1007/s00330-018-5491-2.

Zamani, Hamed, Hamidreza Masjedi, Reza Omidi, and Mohammad Hosein Zare. 2020. 'Establishment of Local Diagnostic Reference Levels for Common Procedures of Computed Tomography in Yazd Province'. *Radiation Protection Dosimetry* 188 (2): 222–31. https://doi.org/10.1093/rpd/ncz279.

Approval letter

Al Quds University
Faculty of Health Professions
Jerusalem –Abu Dis

جامعة القدس
كلية المهن الصحية
القدس – أبو ديس

Research Ethics Subcommittee of Faculty of Health Professions
Letter of approval

May 29, 2021
Ref. No.: RESC/2021-18

Dear Applicants, (**Dr. Mohammad Hjouj, Ms. Hala Rabee**)
Program: **MSc Medical Imaging Department**

The Research Ethics subcommittee of Faculty of Health Professions has recently reviewed your proposal entitled (**Assessment of Organs Absorbed Doses, effective doses and Cancer risk Following HRCT Scan for COVID-19 Patients**) submitted by (**Dr. Mohammad Hjouj**). Your proposal is deemed to meet the requirements of research ethics at Al-Quds University, but further assessment is required by the Central Research Ethics Committee of Al-Quds University. We wish you all best for the conduct of the project.

Hussein ALMasri
Research Ethics Subcommittee Chair
Faculty of Health Professions

Hussein ALMasri

CC: File
CC: Committee members

Appendix 1: Patient data

	A	C	D	E	F	G	H	I	J	K	L	M
1	ID	الجنس	الوزن	الطول	العمر	kVp	mAs	DLP mGy* cm	CTDI mgy	CTDIw	BMI	scan length
2	678836	m	88	170	67	120	250	644.9	17.6	16.509	30.4	36.6
3	2E+06	m	105	192	37	120	250	600	17.6	16.509	28.5	34
4	1E+06	m	85	175	25	120	250	687.2	17.6	16.509	27.8	39
5	1E+06	m	96	175	42	120	250	705.7	17.6	16.509	31.3	40
6	2E+06	m	140	183	30	120	250	930.1	18.7	17.541	41.8	49.7
7	1E+06	f	94	160	48	120	250	659.84	18.2	17.072	36.7	36.2
8	593008	m	80	162	56	120	250	563.21	15.5	14.539	30.5	36.3
9	1E+06	m	85	180	35	120	250	732.14	17.8	16.696	26.2	41.1
10	703799	m	79	164	62	120	250	700.61	18.2	17.072	29.4	38.5
11	558168	m	100	175	61	120	250	480.53	18.6	17.447	32.7	25.8
12	2E+06	m	85	169	67	120	250	579.48	15.5	14.539	29.8	37.4
13	1E+06	m	114	168	49	120	250	637.09	18.2	17.072	40.4	35
14	723679	f	65	170	47	120	250	772.1	17.8	16.696	22.5	43.4
15	2E+06	m	95	182	42	120	250	651.49	17.8	16.696	28.7	36.6
16	884482	m	80	175	47	120	250	467.84	11.6	10.881	26.1	40.3
17	2E+06	m	85	184	49	120	250	549.44	15.5	14.539	25.1	35.4
18	715653	f	85	165	79	120	250	680.62	17.6	16.509	31.2	38.6
19	781178	m	80	175	47	120	250	618.91	15.5	14.539	26.1	39.9
20	1E+06	m	83	172	68	120	250	706.55	18.2	17.072	28.1	38.8
21	719564	m	90	155	89	120	250	719.34	17.6	16.509	37.5	40.8
22	1E+06	m	100	190	41	120	250	679.25	18.2	17.072	27.7	37.3
23	804465	m	80	179	73	120	250	775.48	17.6	16.509	25	44.06
24	505179	m	70	170	66	120	250	722.83	19.3	18.103	24.2	37.45
25	1E+06	m	85	165	32	120	250	694.17	19.3	18.103	31.2	35.96
26	568317	m	97	175	49	120	250	830.21	19.3	18.103	31.7	43
27	744053	m	85	160	59	120	250	544.5	17.6	16.509	33.2	30.9
28	2E+06	f	47	155	32	120	250	1087.35	17.6	16.509	19.6	61.7
29	655314	m	102	176	70	120	250	695.1	17.6	16.509	32.9	39.5
30	658734	f	60	165	49	120	250	1006.8	27	25.326	22	37
31	666572	f	67	169	52	120	250	741.1	19.4	18.197	23.5	38.1
32	717463	m	60	170	63	120	250	728.9	19.3	18.103	20.8	37.8
33	2E+06	f	60	166	68	120	250	532.33	15.5	14.539	21.8	34.3
34	704530	m	90	175	61	120	250	919.6	23.2	21.762	29.4	39.6
35	1E+06	m	65	170	47	120	250	660.79	17.6	16.509	22.5	37.5
36	333572	f	79	160	29	120	250	565.7	17.6	16.509	30.9	32.14
37	729482	f	86	167	46	120	250	687.2	17.6	16.509	30.8	39
38	1E+06	m	57	177	18	120	250	721.41	17.6	16.509	18.2	40.9
39	2E+06	f	75	168	36	120	250	600	17.6	16.509	26.6	34.1
40	2E+06	m	89	175	50	120	250	747.76	17.6	16.509	29.1	42.5
41	2E+06	f	78	163	31	120	250	668.7	17.6	16.509	29.4	37.99
42	2E+06	m	125	195	51	120	250	687.13	17.6	16.509	32.9	39
43	531842	f	87	157	80	120	250	647.6	17.6	16.509	35.3	36.8
44	96356	m	64	174	20	120	250	731.88	17.6	16.509	21.1	41.6
45	531842	f	87	157	80	120	250	589.4	17.6	16.509	35.3	33.4
46	723679	f	65	170	47	120	250	663.32	17.6	16.509	22.5	37.6
47	723679	f	65	170	47	120	250	718.88	17.6	16.509	22.5	40.8
48	558745	f	75	160	56	120	250	552.4	17.6	16.509	29.3	31.3
49	2E+06	f	75	170	65	120	250	655.5	17.6	16.509	26	37.2
50	423147	f	73	162	47	120	250	847.9	17.6	16.509	27.8	48.1

Appendix 2 : VirtualDose-CT software User Interface

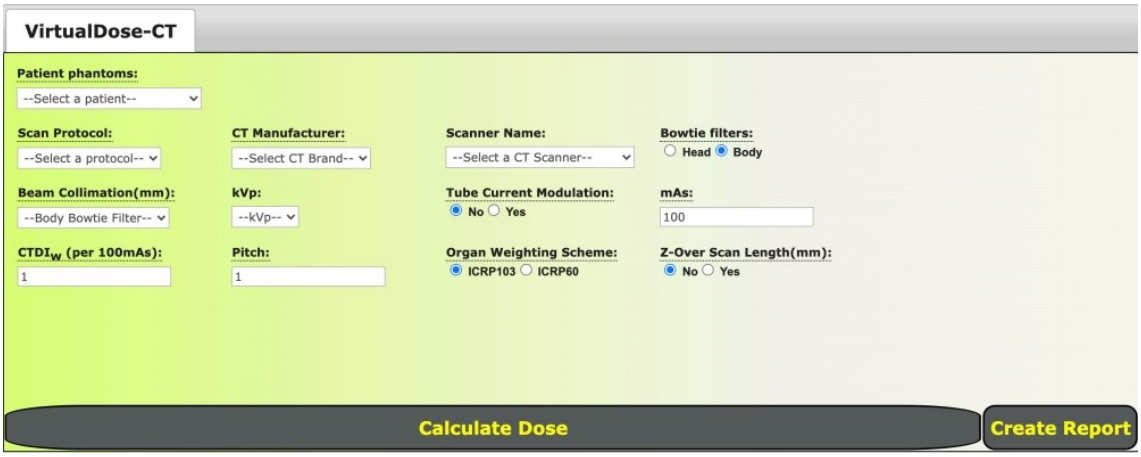

ملخص الدراسة

اعداد: هاله يوسف ربيع

المشرف: د. محمد حجوج

تقييم الجرعات الإشعاعية وخطر الإصابة بالسرطان لمرضى فايروس كورونا بعد اجراء فحص التصوير الطبقي للصدر

التصوير المقطعي المحوسب هو طريقة فعالة لتشخيص مجموعة واسعة من الحالات الطبية. يتفوق التصوير المقطعي المحوسب على الأشعة السينية من حيث توليد الصور وتصوير الأنسجة الرخوة. يعد التصوير المقطعي المحوسب للرئتين أداة تشخيصية مهمة في مكافحة الالتهاب الرئوي. زاد استخدام بروتوكول تصوير الصدر خلال جائحة كوفيد19,حيث يمكن استخدام الأشعة المقطعية كأداة تشخيصية وفحص المرضى المشتبه بهم ولكن يجب النظر في خطر الإشعاع، ويجب تقييم أثار الجرعة الإشعاعية من تصوير الصدر. قد يساعد التصوير المقطعي المحوسب في الكشف المبكر عن مرض الالتهاب الرئوي الخلالي المرتبط بكوفيد-19 , الا انه لا يوجد إجماع على استخدام التصوير المقطعي المحوسب للتشخيص لأن المرحلة الأولى من المرض قد تكون سلبية.

لذلك تهدف هذه الدراسة إلى تقييم تأثير الجرعات الإشعاعية لمرضى كوفيد -19 وسيتم تقييم كل من جرعات الاعضاء والجرعات الفعالة كما سيتم تقدير مخاطر الإصابة بالسرطان الإشعاعي في (الرئة والمعدة والقولون والغدة الدرقية والثدي) المرتبطة بهذه التعرضات وفقا للتقارير BEIR التابعة للأكاديمية الوطنية للعوم في الولايات المتحدة للحماية من الإشعاع، تم تحقيق هدف الدراسة من خلال استخدام التحليل الكمي بأثر رجعي. يتكون مجتمع الدراسة من 48 مريضا بالغا (31 ذكرا 17أنثى)، تتراوح أعمارهم بين 18 و89 عاما، خضعوا لتصوير الصدر الطبقي خلال هذه الفترة. تم جمع البيانات باستخدام نظام محلي لأرشفة الصور والاتصالات، بما في ذلك معلومات المرضى والقياسات البشرية، وكذلك المعلومات الوصفية للجرعة (CTDIv and DLP). تم حساب الجرعة الفعالة باستخدام طريقتين: أولا، باستخدام معامل تحويل الأنسجة

للتصوير المقطعي المحوسب للصدر، وثانيا، باستخدام برنامج التصوير المقطعي المحوسب، والذي يحسب أيضا الجرعة الممتصة للأعضاء ويستند البرنامج على قاعدة بيانات كبيرة من جرعات الجهاز ولدت عن طريق نظام محاكاة مونت كارلو (MC) باستخدام مكتبة من 25 من المجسمات. ثم تم تحديد خطر الإصابة بالسرطان في عضو معين من خلال معاملات الخطر التي تم الحصول عليها من(BEIR VII). يتم تعريف كل معلمة قياس الجرعات بالمتوسط والقيمة المتوسطة والانحراف المعياري والنسبة المئوية 75. استخدمنا المتوسط لمقارنة بياناتنا بالقيم المنشورة. كما تم تحديد القيمة المتوسطة للجرعات المكافئة واحتمال خطر الإصابة بالسرطان للأعضاء لكل من المجموعات الفرعية بين الجنسين تم استخدام اختبار ترتيب رتبة سبيرمان لاختبار الارتباطات بين .DLP\BMI, EDDLP, EDMC تم تعريف مستوى الأهمية على أنه < 0.05

وكشفت نتائج الدراسة أن متوسط الجرعة الفعالة المحسوبة لمجموع السكان 9.7 ملي سيفرت، ومتوسط الجرعة الفعالة المقدرة ببرامج التصوير المقطعي المحوسب للجرعة الافتراضية كان 13.47 ملي سيفرت، مع متوسط جرعة الإناث أعلى من الذكور بقيمة 14.75 و12.7 ملي سيفرت على التوالي. وأظهرت النتيجة انخفاض الجرعة الفعالة للمرضى الذين يعانون من زيادة مؤشر كتلة الجسم المريض وتزداد مع زيادة DLP أظهرت الإناث جرعات أعضاء أعلى من الذكور لجميع الأعضاء وبالتالي خطر اعلى للإصابة بالسرطان والتي كانت أعلى في الرئتين لكلا الجنسين حيث كانت 51.6 لكل 100.000 للإناث و21.8 لكل 100.000 للذكور. ونستنتج أن بروتوكول تصوير الصدر الحالي يؤدي إلى جرعات إشعاعية كبيرة للمرضى مقارنة مع ما ذكرت في دراسات اخرى.